Discovery and Cross-Section Measurement of Neutron-Rich Isotopes in the Element Range from Neodymium to Platinum at the FRS

J. Kurcewicz[a,*], F. Farinon[a,b,**], H. Geissel[a,b], S. Pietri[a], C. Nociforo[a], A. Prochazka[a,b], H. Weick[a], J.S. Winfield[a], A. Estradé[a,c], P.R.P. Allegro[d], A. Bail[e], G. Bélier[e], J. Benlliure[f], G. Benzoni[g], M. Bunce[h], M. Bowry[h], R. Caballero-Folch[i], I.Dillmann[a,b], A. Evdokimov[a,b,j], J.Gerl[a], A. Gottardo[k], E. Gregor[a], R. Janik[l], A. Kelić-Heil[a], R. Knöbel[a], T. Kubo[m], Yu. A. Litvinov[a,n], E. Merchan[a,o], I. Mukha[a], F. Naqvi[a,p], M. Pfützner[1], M. Pomorski[1], Zs. Podolyák[h], P.H. Regan[h], B. Riese[a,b], M.V. Ricciardi[a], C. Scheidenberger[a,b], B. Sitar[l], P. Spiller[a], J. Stadlmann[a], P. Strmen[l], B. Sun[b,r], I. Szarka[l], J. Taïeb[e], S. Terashima[a,m], J.J. Valiente-Dobón[k], M. Winkler[a], Ph. Woods[s]

[a] *GSI Helmholtzzentrum für Schwerionenforschung, 64291 Darmstadt, Germany*
[b] *Justus-Liebig-Universität Gießen, 35392 Gießen, Germany*
[c] *Astronomy and Physics Department, Saint Mary's University, Halifax, Nova Scotia B3H 3C3, Canada*
[d] *Institute of Physics, Universidade de São Paulo, CEP 05508-090 Cidade Universitária, São Paulo, Brazil*
[e] *CEA DAM DiF, 91290 Arpajon Cedex, France*
[f] *Universidad de Santiago de Compostela, E-15706 Santiago de Compostella, Spain*
[g] *INFN sezione di Milano, I-20133 Mialno, Italy*
[h] *Department of Physics, University of Surrey, Guildford, Surrey, UK GU2 7XH*
[i] *Universitat Politècnica de Catalunya, 08034 Barcelona, Spain*
[j] *National Research Tomsk Polytechnic University, Tomsk 634050, Russia*
[k] *INFN - Laboratori Nazionali di Legnaro, 35020 Legnaro, Italy*
[l] *Faculty of Mathematics and Physics, Comenius University, 842 48 Bratislava, Slovakia*
[m] *RIKEN Nishina Center, RIKEN, Wako, Saitama 351-0198, Japan*
[n] *Max-Planck-Institut für Kernphysik, 69117 Heidelberg, Germany*
[o] *Institut für Kernphysik, Technische Universität Darmstadt, 62289 Darmstadt, Germany*
[p] *Institut für Kernphysik,Universität zu Köln, 50937 Köln, Germany*
[q] *Faculty of Physics, University of Warsaw, 00-681 Warsaw, Poland*
[r] *School of Physics and Nuclear Energy Engineering, Beihang University, Beijing 100191, China*
[s] *School of Physics, University of Edinburgh, Edinburgh EH9 3JZ, UK*

Abstract

With a new detector setup and the high-resolution performance of the fragment separator FRS at GSI we discovered 57 new isotopes in the atomic number range of $60 \leq Z \leq 78$: $^{159-161}$Nb, $^{160-163}$Pm, $^{163-166}$Sm, $^{167-168}$Eu, $^{167-171}$Gd, $^{169-171}$Tb, $^{171-174}$Dy, $^{173-176}$Ho, $^{176-178}$Er, $^{178-181}$Tm, $^{183-185}$Yb, $^{187-188}$Lu, ^{191}Hf, $^{193-194}$Ta, $^{196-197}$W, $^{199-200}$Re, $^{201-203}$Os, $^{204-205}$Ir and $^{206-209}$Pt. The new isotopes have been unambiguously identified in reactions with a ^{238}U beam impinging on a Be target at 1 GeV/u. The isotopic production cross-section for the new isotopes have been measured and compared with predictions of different model calculations. In general, the ABRABLA and COFRA models agree better than a factor of two with the new data, whereas the semiempirical EPAX model deviates much more. Projectile fragmentation is the dominant reaction creating the new isotopes, whereas fission contributes significantly only up to about the element holmium.

Key words: NUCLEAR REACTIONS Be(^{238}U,X), $E = 1$ GeV/u; measured Nb-Pt fragments isotopic production σ; Comparison with previous results and model predictions.

1. Introduction

Heavy neutron-rich nuclides are of great interest for nuclear astrophysics and basic nuclear spectroscopy. This becomes immediately obvious when one looks at the predicted path for r-process nuclei and their decay. The study of shell evolution far off stability and towards the expected magic numbers N=82, 126 and thus the waiting points of the r-process nuclides are of interest for both fields. The accurate knowledge of the atomic masses and lifetimes are essential for the understanding of the nucleosynthesis [1, 2, 3]. Presently, the corresponding theories when applied to newly opened experimental territories still deviate significantly from the results of measurements.

Experimentally the area of heavy neutron-rich nuclides is difficult to reach because of the low production cross-sections and the great challenge of separation and isotopic identification. Relativistic energies of the reaction products and the high ion-optical resolution of the in-flight separator FRS [4] are the keys to the frontiers in this domain of nuclides. High velocities are required to reduce the number of populated ionic charge-states for each element, mainly to bare fragments with a low contamination of H- and He-like ions.

Several milestones in nuclear physics have been achieved with the FRS, like the discovery and spectroscopy of the double magic nuclei ^{100}Sn [5, 6] or the discovery of 2p radioactivity in ^{45}Fe [7]. In the pioneering experiments with uranium projectile fission with the FRS at 750 MeV/u more than 120 new isotopes have been discovered, among them ^{78}Ni [8]. These achievements have launched a new research activity for fission studies [9] and an area of applied physics towards accelerator-driven reactors and nuclear-waste transmutation [10]. Owing to the success of in-flight fission at high energies, all next-generation in-flight exotic nuclear beam facilities include the production via projectile fission. For example, very recently the new powerful Radioactive Ion Beam Factory (RIBF) in RIKEN has successfully started the experimental program with the discovery of new isotopes in the atomic number range of $26 \leq Z \leq 56$ produced via in-flight fission of an intense ^{238}U beam [11]. The search for the neutron dripline at low Z has been a major research activity at GANIL (France)[12], NSCL (USA)[13] and RIKEN (Japan)[14, 12] for many years. At the NSCL facility at MSU (USA) new neutron-rich isotopes have been observed via reactions with a ^{48}Ca and ^{76}Ge beam at about 140 MeV/u [15, 13].

In the recent years, the intensity for ^{238}U beams provided by the GSI accelerators have increased almost by a factor 10, which has opened new perspectives for the production and study of the heaviest projectile fragments [16, 17]. Even along with mass measurements at the FRS-ESR facility new isotopes have been observed [20, 17]. The fragmentation reaction of ^{208}Pb seems also to be very promising for production of neutron-rich isotopes as it has been proven in the recent FRS experiments [18, 19].

In this letter we report on the discovery of 57 new neutron-rich isotopes in the element range of Nd to Pt at the FRS by the use of new particle identification methods [21].

2. Experimental technique

The experiment was performed with the SIS-18 synchrotron of GSI Darmstadt, which delivered a 1 GeV/u ^{238}U beam in spills lasting 0.5-2 s with a repetition period of 2-4 s. The beam impinged on a 1.6 g/cm^2 thick beryllium target placed at the entrance of the projectile FRragment Separator (FRS) [4]. The primary beam intensity was of the order of 2×10^9 ions/spill. The ^{238}U intensity was recorded by a calibrated secondary-electron transmission monitor [22]. The reaction products were separated by the FRS operated in an overall achromatic ion-optical mode. A schematic view of the FRS and the experimental setup is shown in Fig. 1. The spatial separation in flight was achieved by twofold application of the $B\rho$-ΔE-$B\rho$ method, i.e., the atomic energy losses in two degraders, located at the first (F1) and second (F2) focal planes, were measured via magnetic rigidity analysis. In this way, the reaction products are spatially separated and by the

*Corresponding author; electronic address: j.kurcewicz@gsi.de

**Part of PhD work, Justus-Liebig University, Gießen, 2011

use of various detectors their nuclear charge Z and mass number A could be determined. After the first magnetic selection and the 2.5 g/cm^2 thick aluminum degrader at F1, the reaction products were slowed down in an aluminium disk degrader located at the intermediate focal plane F2. With the disk angle the degrader shape was tuned to preserve the achromatism. Even at these relativistic velocities the atomic charge states of the heavy fragments represent a separation problem. Therefore, medium Z-material niobium foils were placed both behind the target and the F2-degrader to enhance the yield of bare fragments. The thicknesses of these electron strippers were 223 mg/cm^2 for the first and 106 mg/cm^2 for the latter. The total thickness of the F2-materials including detectors was 1.43 g/cm^2 aluminium equivalent.

The complete particle identification in-flight was performed on an event-by-event basis with time-of-flight (ToF), energy-deposition ($\Delta E'$) and magnetic rigidity measurements (ToF-$\Delta E'$-$B\rho$ method). The ToF measurement was performed with two plastic scintillator detectors, one located at F2 and the other one at the final focal plane (F4). The flight path was about 37 m between the two detectors. The ToF value for the selected isotopes was of the order of 160 ns in the laboratory frame. At the exit of the FRS, two ionization chambers (MUSIC) filled with P10 gas at 1 atm. pressure were mounted with a 104 mg/cm^2 copper stripper placed in between. The MUSIC detectors [23] delivered the energy-deposition signals of fragments, thus providing the information of their atomic numbers. The velocity dependence of the penetrating ions was taken into account before the energy-deposition signal was applied for Z identification. The magnetic rigidity measurements were performed with four time-projection chambers (TPC), two located at the dispersive focal plane (F2) and two others mounted at the exit of the FRS. The TPC provided full tracking information (angle and position) for the transmitted fragments. The event-by-event identification, and thus also the in-flight separation, were verified by the isomer tagging technique [21]. In the range of the particle identification spectrum, known μs isomers were selected (^{171m}Tm, ^{172m}Yb and ^{175m}Lu) whose gamma rays were recorded in coincidence with the incoming ions. With these multiple redundant measurements and the two-stage in-flight separation criteria, we achieved an unambiguous isotope identification. Finally, a range selection was applied in addition because the selected fragments were stopped in a layer of matter viewed either by the RISING germanium detector setup [24], composed of fifteen Euroball cluster of seven crystals used in 4π configuration, or the simpler isomer tagging device [21], which consisted of the two electromechanically cooled Ge detectors, a stopper foil, and a veto scintillation counter.

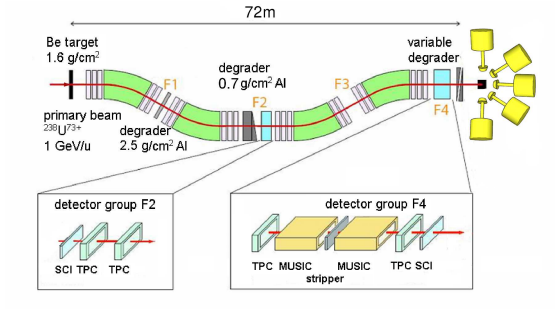

Figure 1: (color online) Schematic view of the FRS and the experimental setup. The magnetic dipole and quadrupole magnets of the FRS and the target and different focal-plane areas are depicted. The different energy degraders at the focal planes F1, F2, and F4 are schematically shown. The detector setups placed in the central and final focal planes are shown as zoomed inserts in the picture. After identification in flight the ions are stopped in an implantation detector viewed by a gamma detector array.

3. Data analysis

In the experiment four different $B\rho$ settings of the FRS were applied, which were chosen to yield optimum intensities for bare ^{172}Dy, ^{194}Os, ^{198}Os and ^{202}Os ions, i.e., the magnetic fields were selected to center these isotopes during their travel inside the FRS system. The data collected in each setting were processed by the following procedure based on a combination of ToF, position and energy-deposition.

In the first step of analysis a two-dimensional plot of the energy deposition in the first MUSIC detector

as a function of the energy deposition signal from the second MUSIC was created. Only bare ions in both detectors were chosen for further analysis, thus rejecting ions with different charge states in both MUSICs or secondary reaction products created in the detector material.

In the second step, a distribution of the reconstructed nuclear charge as a function of the energy loss of the ions in the degrader located at F2 was created. This allowed a clear identification of the group of ions which did not change their charge state while penetrating the matter placed at F2.

Unambiguous isotope identification requires an additional selection based on the ions' position at the final focus ($B\rho$), energy deposition signals in both scintillators and a correlation between the measured angles at the intermediate and final focal planes. The latter condition reflects the ion-optical image conditions which are needed also for the correct $B\rho$ determination. An example of the final isotope identification plot is shown in Fig. 2. The projection of this plot on the A/q axis selecting every element covered in the $B\rho$ settings is given in Fig. 3

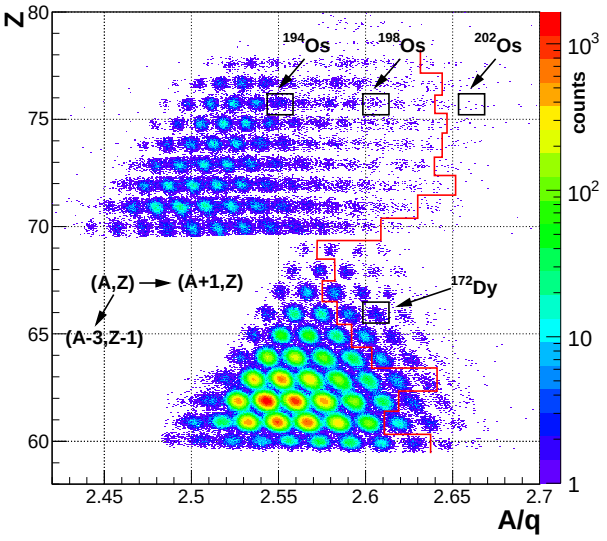

Figure 2: (color online) Identified atomic number Z of the incoming ions as a function of their A/q ratio, at the final focal plane (F4). In the A/q ratio, the time-of-flight and magnetic rigidity analysis information is included. The plot shows the superimposed data acquired in all $B\rho$ settings. The solid line shows the border of hitherto unobserved isotopes, i.e., the discovered new isotopes are on the right hand side of the border line. The black rectangles show the group of ions corresponding to the $B\rho$ setting of the spectrometer.

4. Production cross-sections

The data recorded for each $B\rho$ setting were analyzed by the described procedure to achieve an unambiguous isotope identification. In the next step the production cross-sections of individual isotopes were determined according to:

$$\sigma_f = \frac{N_f}{T_{opt} T_{sec} P_0 Y N_p f_{dt}}, \qquad (1)$$

where N_f is the number of registered ions of a certain isotope, T_{opt} the ion-optical transmission, T_{sec} a correction for secondary reactions in the matter placed after the target (e.g., degraders and detectors), P_0 the probability that an ion remains fully stripped in both stages of the separator, Y the correction for losses of primary beam and fragments due to nuclear reactions in the target material, N_p the total number of ^{238}U ions and f_{dt} the correction for the dead-time losses of the data acquisition system. All secondary reactions in the target and the matter in the focal planes are taken into account by applying the Benesh-Cook-Vary formula [25].

Calculations of charge-state distributions were performed for the heavy fragments of interest with the CHARGE code [26] yielding P_0 values in the range of 0.9 and 0.6 for Nd-Pt isotopes, respectively. The ion-optical transmissions T_{opt} have been calculated by using the Monte-Carlo simulation program MOCADI [27, 28] assuming the kinematics of projectile fragmentation [35]. The transmission values were obtained separately for each $B\rho$ setting. The typical T_{opt} values were of the order of 0.4-0.6 for isotopes with A/q close to the reference setting of each FRS setting. This relative small value is due to the tight slits settings of the FRS which were applied in order to decrease the number of contaminants, mainly light

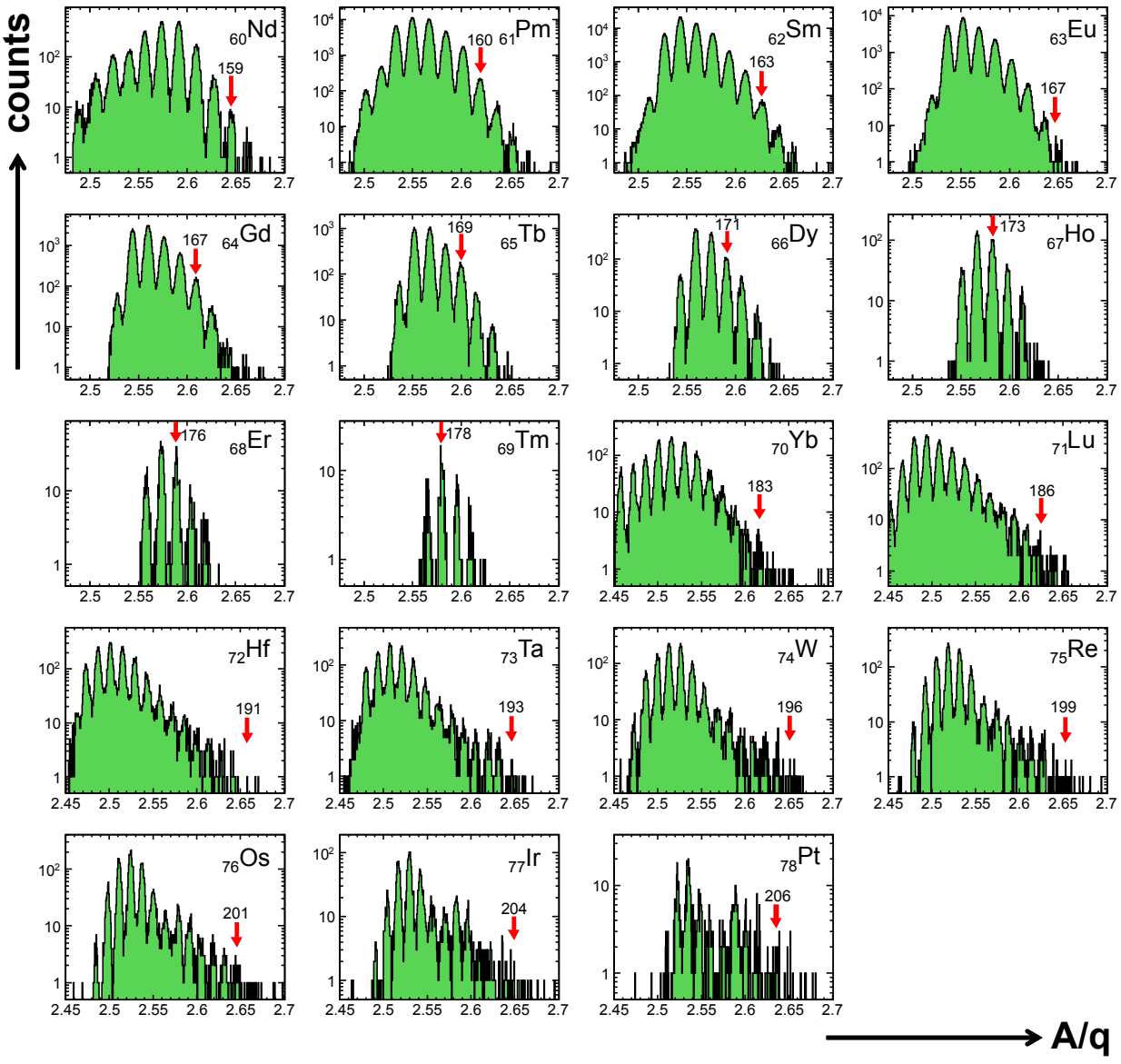

Figure 3: (color online) Projection of the identification plot shown on Fig. 2 constructed for all elements covered by the different $B\rho$ settings of the FRS. For each element the arrow indicates the lightest of the isotopes (marked by the mass numbers) observed for the first time.

fission fragments (Z<60), reaching the F4 area.

5. Results

In this experiment we discovered 57 new isotopes with atomic numbers in the range $60 \leq Z \leq 78$: $^{159-161}$Nb, $^{160-163}$Pm, $^{163-166}$Sm, $^{167-168}$Eu, $^{167-171}$Gd, $^{169-171}$Tb, $^{171-174}$Dy, $^{173-176}$Ho, $^{176-178}$Er, $^{178-181}$Tm, $^{183-185}$Yb, $^{187-188}$Lu, ^{191}Hf, $^{193-194}$Ta, $^{196-197}$W, $^{199-200}$Re, $^{201-203}$Os, $^{204-205}$Ir and $^{206-209}$Pt and measured their production cross section. The new isotopes have been unambiguously identified in flight by applying a two-fold $B\rho$-ΔE-$B\rho$ separation scenario and redundant ToF-$\Delta E'$-$B\rho$ analysis using new detector systems [21]. The observed new isotopes are presented for the different elements in Fig. 3. For each element the arrow indicates the lightest of the isotopes observed for the first time. For all isotopes discovered in this work we can set a lower limit of half-life to 300 ns which corresponds to the time of flight between the production target and F4.

The isotopic production cross-section have been determined in this experiment down to the pico-barn level. Particularly, the steep descent of the yields of the neutron-rich isotopes has been mapped. The cross-section obtained for the production of Nd-Pt isotopes are shown in Fig. 4 and listed in Table 1. The error bars are mainly determined by the statistics due to tiny production cross-sections, partially due to the low transmission of isotopes characterized with a Bρ value far from the central field setting with respect to the optical axis. The latter aspect has been partially taken care of by the different field settings applied in these measurements. The measured cross-sections in this experiment represent the outskirts of the chart of nuclides. Therefore, it is obvious that the present results cannot be compared with previous experimental data. However, a good orientation for the consistencies of the cross-section evolution can be obtained with the comparison to results from previous experimental studies [30, 31]. Although the latter data from the literature are obtained from reactions of 1 GeV/u ^{238}U beam with a liquid hydrogen target the continuous transition of the two experimental data sets is remarkable. The excitation in the reaction with hydrogen target nuclei should be lower than in our case with a beryllium target but this plays obviously a minor role for the compared fragment distribution in the overlap region. Our cross-section are compared with calculations based on the ABRABLA [32] and COFRA [33] models and shown in Fig. 4. The ABRABLA model is an improved abrasion-ablation model which takes also into account microscopic structural effects and the contribution of fission. COFRA and EPAX have both the fission process not included. The predictions of the semiempirical EPAX parametrization [34] are given as well.

Since ABRABLA is a Monte-Carlo code, a long computation time is required to reach very-low production cross-section. Thus COFRA, the analytical version of the abrasion-ablation model, was used for the most neutron-rich nuclei. The predictions of ABRABLA show an overall good agreement with the experimental data. The used version of the code involves fission as a possible deexcitation step of the created prefragment. The lighter isotopes in the element range Nb-Dy show a significant contribution from the fission process which starts to play a minor role for heavier nuclei investigated in this work. The latter statement was deduced from the ABRABLA calculation and is also visible by the underestimation of EPAX, which takes into account only projectile fragmentation.

The COFRA model agrees well with the experimental data, however, a small gradual deviation between results of the measurements and the model predictions can be observed for the heaviest (Os-Pt) nuclei. For most of the cases the overestimation is less than a factor of two compared with the measured values which means it is well suited to make valid predictions for new studies in this field of neutron-rich isotopes. The EPAX predictions largely overestimates the production cross-sections in the region of neutron-rich nuclei in the element range of Yb to Pt. This reflects the present limitation of that semiempirical model with its parametrization based on previous data, hence our results could be a base for a new parametrization of EPAX.

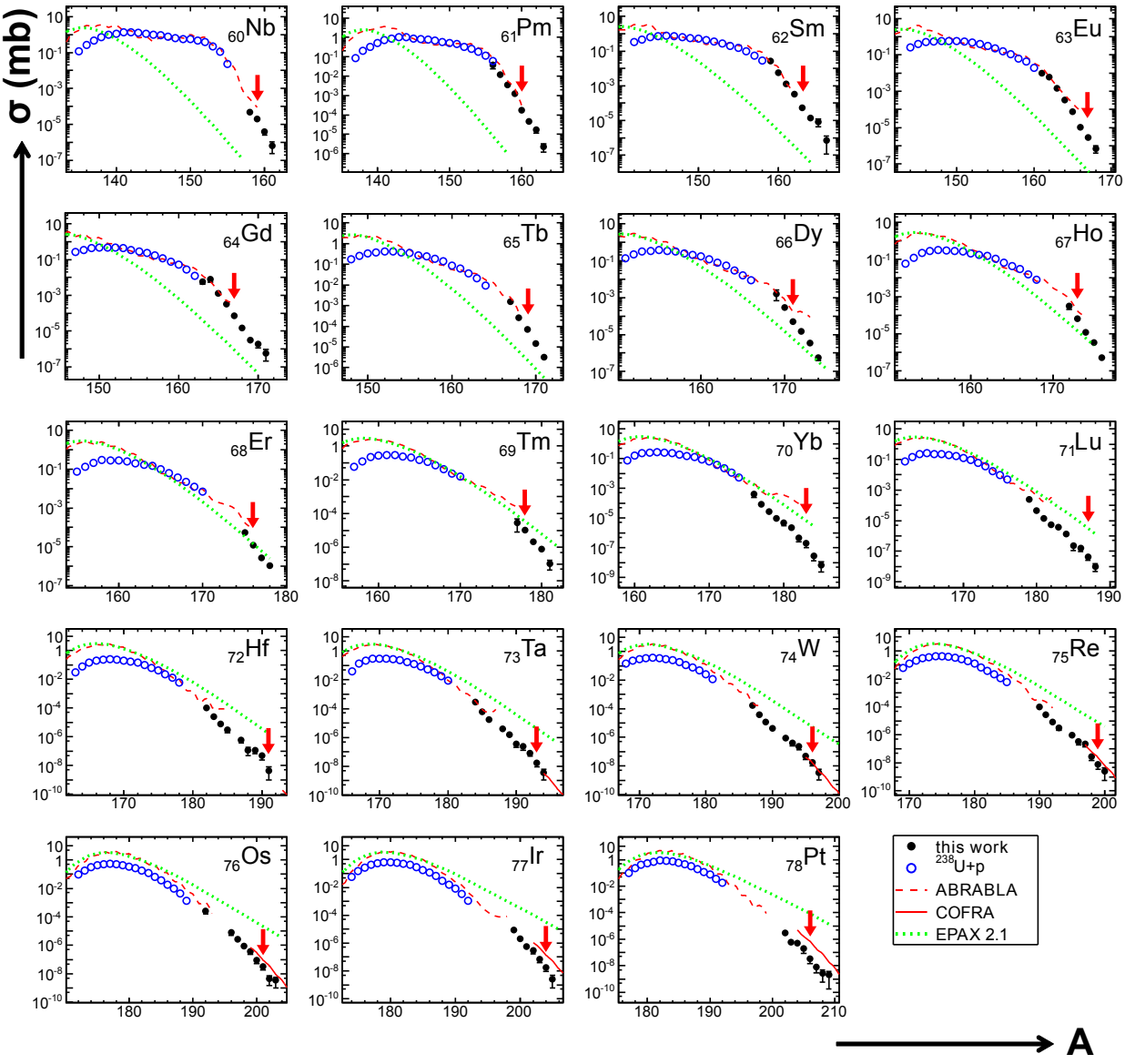

Figure 4: (color online) Measured production cross-sections of fragments produced in the reaction ^{238}U (1 GeV/u) + Be (black circles), shown together with the experimental results obtained by Bernas et al. [29] ($Z = 60 - 64$), [30] ($Z = 65 - 73$) and Taïeb et al. [31] ($Z = 74 - 78$) in the reaction ^{238}U (1 GeV/u) + p (blue open circles). The red dashed line represents the predictions of the ABRABLA model [32] and the continuous red line shows the results of COFRA [33] ($Z = 73 - 78$). The green dotted line shows the prediction of EPAX model [34]. For each element the arrow indicates the lightest of the isotopes observed for the first time.

Table 1: Production cross-section of new isotopes measured in this work in reaction 1 GeV/u ^{238}U on Be.

Isotope	σ(nb)	Isotope	σ(nb)	Isotope	σ(nb)	Isotope	σ(nb)
^{159}Nb	20(6)	^{169}Gd	3.2(5)	^{177}Er	2.7(0.3)	^{197}W	0.0034(17)
^{160}Nb	3.9(1.4)	^{170}Gd	1.9(8)	^{178}Er	1.1(2)	^{199}Re	0.0076(27)
^{161}Nb	0.7(4)	^{171}Gd	0.6(4)	^{178}Tm	10.6(1.8)	^{200}Re	0.0025(14)
^{160}Pm	180(15)	^{169}Tb	71(4)	^{179}Tm	2.1(3)	^{201}Os	0.033(7)
^{161}Pm	45(6)	^{170}Tb	14.6(1.1)	^{180}Tm	0.79(17)	^{202}Os	0.0044(2)
^{162}Pm	17(6)	^{171}Tb	3.3(0.4)	^{181}Tm	0.11(6)	^{203}Os	0.0035(17)
^{163}Pm	2.2(1.0)	^{171}Dy	49(3)	^{183}Yb	0.21(6)	^{204}Ir	0.017(5)
^{163}Sm	53(4)	^{172}Dy	15.0(1.1)	^{184}Yb	0.028(9)	^{205}Ir	0.0026(15)
^{164}Sm	14(2)	^{173}Dy	3.5(4)	^{185}Yb	0.007(3)	^{206}Pt	0.033(11)
^{165}Sm	8.3(4)	^{174}Dy	0.57(18)	^{187}Lu	0.043(9)	^{207}Pt	0.008(3)
^{166}Sm	0.7(5)	^{173}Ho	65(6)	^{188}Lu	0.010(3)	^{208}Pt	0.0027(15)
^{167}Eu	2.9(7)	^{174}Ho	12(1)	^{191}Hf	0.0043(25)	^{209}Pt	0.0020(14)
^{168}Eu	0.7(3)	^{175}Ho	3.4(4)	^{193}Ta	0.017(5)		
^{167}Gd	71(4)	^{176}Ho	0.51(14)	^{194}Ta	0.0037(19)		
^{168}Gd	14.9(1.2)	^{176}Er	1.19(12)	^{196}W	0.018(4)		

6. Summary

The results of the present experiment opens a new field for nuclear spectroscopy and also for nuclear astrophysics in the heavy nuclei range. With a new detector setup and the high-resolution performance of the fragment separator FRS we discovered 57 new isotopes in the atomic number range of $60 \leq Z \leq 79$. The new isotopes have been unambiguously identified in projectile fragmentation reactions with a ^{238}U beam at 1 GeV/u. The isotopic production cross-section for the new isotopes have been measured and compared with the predictions of the ABRABLA, COFRA, and EPAX models. In general, with COFRA a good overall agreement has been achieved to be confident for reliable predictions in unknown territory. The next steps in this experimental campaign will be half-life and mass measurements, as well as decay spectroscopy after implantation in silicon detectors.

7. Acknowledgement

It is a pleasure to thank the technical staffs of the accelerators, the FRS, and the target laboratory for their valuable contribution to the beam quality and experimental setups. The authors gratefully acknowledge fruitful discussions with G. Martinez-Pinedo, K. Otsuki and B. Pfeiffer. This work was supported by STFC (UK). B.Sun is partially supported by NECT and NSFC 11105010.

References

[1] F. Käppeler, F.K. Thielemann, and M. Wiescher, Ann. Rev. Part. Nucl. Science 48, (1998) 175.

[2] B. Franzke, H. Geissel and G. Münzenberg, Mass Spectrom. Rev. 27(5) (2008) 428.

[3] Roederer et al., ApJ 698, (2009) 1963.

[4] H. Geissel, et al., Nucl. Instrum. Methods Phys. Res. B 70 (1992) 286.

[5] R. Schneider et al., Z. Phys. A 348 (1994) 241.

[6] C.B. Hinke, PhD. Thesis, Technische Universität, München 2010.

[7] M. Pfützner, Eur. Phys. J. A 14 (2002) 279.

[8] C. Engelmann et al., Z. Phys. A 352 (1995) 351.

[9] K-H Schmidt, et al., Nucl. Phys. A 665 (2000) 221.

[10] J. Benlliure, et al., AIP Conf. Proc. "Experimental Nuclear Physics in Europe: Facing the next millenium", 495 (1999) 458.

[11] T. Ohnishi et al., Journal of the Physical Society of Japan 79 (2010) 201.

[12] S. Lukyanov et al., J. Phys. G 28 (2002) L41.

[13] O. Tarasov et al., PRC 75 (2007) 064613, O. Tarasov et al., Phys. Rev. Lett. 102 (2009) 142501.

[14] H. Sakurai et al., Phys. Lett. B 448 (1999) 180.

[15] T. Baumann et al., Nature 449 (2007) 1022.

[16] H. Alvarez-Pol et al., Phys. Rev. C 82 (2010) 041602(R).

[17] L. Chen et al., Phys. Lett. B 691, 234 (2010).

[18] T. Kurtukian-Nieto et al., Proceedings of the IX Int. Symposium on Nuclear Astrophysics - Nuclei in the Cosmos, 25-30 June 2006, CERN, Geneva, PoS(NIC-IX)008 (2006).

[19] T. Kurtukian-Nieto et al., J Phys. Conf. Series 202 (2010) 012012.

[20] H. Geissel et al., Eur. Phys. J.-Spec. Top. 150 (2007) 109.

[21] F. Farinon, PhD Thesis, Justus Liebig University Giessen 2011.

[22] B. Jurado, K.-H. Schmidt, K.-H. Behr, Nucl. Instrum. Methods Phys. Res. A 483 (2002) 603.

[23] A. Stolz et al., GSI Sicentific Report 1998, p. 174.

[24] S. Pietri et al., Nucl. Instrum. Methods Phys. Res. B 261 (2007) 1079.

[25] C. Benesh, B. Cook, J. Vary, Phys. Rev. C 40 (1989) 1198.

[26] C. Scheidenberger, et al., Nucl. Instrum. Methods Phys. Res. B 142 (1998) 441.

[27] N. Iwasa et al., Nucl. Instrum. Methods Phys. Res. B 126 (1997) 284.

[28] http://www-linux.gsi.de/~weick/mocadi.

[29] M. Bernas, et al., Nucl. Phys. A 725 (2003) 213.

[30] M. Bernas, et al., Nucl. Phys. A 765 (2006) 197-210.

[31] J. Taieb, et al., Nucl. Phys. A 724 (2003) 413-430.

[32] J.-J. Gaimard, K.-H. Schmidt Nucl. Phys. A 531 (1991) 709.

[33] J. Benlliure et al., Nucl. Phys. A 660 (1999) 87.

[34] K. Sümmerer and B. Blank, Phys. Rev. C 61 (2000) 034607 (2000).

[35] D.J. Morrissey, Phys. Rev. C 39 (1989) 460.